COMPDYN 2021
8th ECCOMAS Thematic Conference on
Computational Methods in Structural Dynamics and Earthquake Engineering
M. Papadrakakis, M. Fragiadakis (eds.)
Streamed from Athens, Greece, 27—30 June 2021

OPTIMAL LATERAL RESISTING SYSTEMS FOR HIGH-RISE BUILDINGS UNDER SEISMIC EXCITATIONS

Giulia Angelucci[1], Giuseppe Quaranta[2], and Fabrizio Mollaioli[1]

[1]Department of Structural and Geotechnical Engineering, Sapienza University of Rome
via Gramsci 53, 00197 Rome, Italy
e-mail: {giulia.angelucci,fabrizio.mollaioli}@uniroma1.it

[2] Department of Structural and Geotechnical Engineering, Sapienza University of Rome
via Eudossiana 18, 00184 Rome
e-mail: giuseppe.quaranta@uniroma1.it

Keywords: Lateral bracing system, Seismic design, Stochastic optimization, Tall building, Topology optimization.

Abstract. *It is generally presumed that the design of tall buildings is mainly dictated by wind loads rather than seismic actions because of the high flexibility and, therefore, long natural periods. However, slender buildings exhibit a complex dynamic behavior, and the involvement of higher modes can result in higher flexural and shear demands than expected. Overlooking the importance of strength, stiffness, and stability requirements in seismic design of tall buildings can thus leads to excessive damage, large residual deformations, and even failure. In this regard, since pure rigid frames alone are not sufficient to withstand lateral loads, as those due to earthquakes, bracing systems are often introduced to stiffen the steel frameworks of tall buildings. The design of lateral bracing systems, in turn, calls for the selection of a suitable pattern for the diagonals arrangement, which is commonly performed through trial-and-error procedures that can require many iteration cycles. It is too evident that this approach does not neither ensure the convergence towards a design solution able to fulfill all requirements, nor the achievement of an optimal solution that minimizes the consumption of structural material and thus the total construction costs. In this context, topology optimization might represent an effective tool for improving the design of tall buildings under earthquake. Therefore, a topology optimization methodology is here presented to support the selection of the most effective design solution for the lateral bracing systems of tall buildings, in such a way to meet minimum weight requirement while ensuring the highest structural performance. Specifically, a density-based approach is adopted to establish an optimization design procedure able to generate optimal lateral-resisting systems for tall buildings subjected to earthquakes. The optimum design is formulated in terms of minimum compliance, also to facilitate the comparison of the material distribution results with those already available in the literature. Numerical results presented in this work are concerned with two-dimensional case studies, which are envisioned as part of realistic tall buildings.*

1 INTRODUCTION

The introduction of automated optimization approaches has demonstrated great potential in assisting designers to achieve more efficient and advanced structural systems than those obtained using traditional iterative procedures. Specifically, topology optimization has attracted significant attention in the last decades as a robust computational tool for the identification of high-performing design solutions at reduced material consumption. Efficiency and effectiveness of topology optimization for defining bracing systems in multi-story buildings has been widely demonstrated in recent research works, most of which refer to wind loading within deterministic frameworks [1–5].

Although interesting results have been successfully achieved under static loading conditions, slender buildings exhibit a complex dynamic behavior where the involvement of higher modes can result in high flexural and shear demands. To this end, a great effort has been devoted to incorporate the topology optimization problem in a dynamic setting. Previous attempts targeted at enhancing the dynamic performance of structural systems through topology optimization have addressed the maximization of the natural eigenfrequencies of structures under free vibration [6–9] and the minimization of the dynamic compliance [10–12]. Because element-wise design variables operate on both stiffness and self-mass of the continuum domain, the mitigation of the overall dynamic response can be properly performed within a topological optimization approach via density-based formulations. However, it is easy to observe that optimizing the topology of large-scale models, as the case of tall buildings, inevitably involves a huge number of degrees of freedom. Hence, the limitations associated with the use of computationally expensive finite element models have led recently to the implementation of model reduction techniques based on modal decomposition methods [13–15]. In dynamic topology optimization problems, the seismic ground motion is usually modeled as stochastic process using the random vibration theory. In most of the existing works, seismic loading conditions are commonly simulated using a stationary Gaussian-type stochastic excitation whereas the design criterion is concerned with the compliance minimization [16–18] or the strain energy minimization [19].

This paper presents a computational framework for the minimization of the dynamic compliance in linear elastic multi-story buildings subjected to seismic ground motion. The optimization procedure integrates the random vibration theory together with the Solid Isotropic Material with Penalization (SIMP) technique whereas a gradient-based optimizer is employed for updating the design variables. Particularly, the use of the random vibration theory offers several advantages as compared to traditional time-history analyses since it allows to perform iterative optimization procedures at affordable computational cost. Compared to response analysis based on integration schemes in the time domain, in fact, this allows to speed up the optimization routines while accurately identifying the stochastic features of the seismic behavior of the building without performing time consuming Monte Carlo simulations. Finally, numerical examples are presented to demonstrate the influence of the mass modeling on the final topologies. The applicability of the formulation within topology optimization procedures as well as stability and effectiveness of the proposed approach in finding the optimum solutions are discussed with reference to a paradigmatic case study. Mesh independent solutions are monitored by operating a gradual refinement of the mesh structure over the design domain.

2 OPTIMUM DESIGN UNDER DETERMINISTIC CONDITIONS

This work is meant to optimize the lateral loading resisting systems for seismically excited large structures by means of topology optimization. For a better understanding of the optimiza-

tion problem, the topology optimization problem in static and dynamic settings are sequentially discussed henceforth.

For a linear elastic structure with a continuous domain discretized into n_d degrees of freedom and n_f finite elements, the most common topology optimization problem formulation in case of static loads aims at minimizing the compliance of the structural system under volume constraints, that is:

$$\begin{aligned} &\min_{\boldsymbol{\rho}} \left\{ \mathbf{u}^\top \mathbf{K} \mathbf{u} \right\} \\ &\text{s.t.} \\ &\sum_{e=1}^{n_f} V_e = V_{max} \\ &\boldsymbol{\rho}_\ell \leq \boldsymbol{\rho} \leq \boldsymbol{\rho}_u, \end{aligned} \tag{1}$$

where V_e is the volume of the generic finite element e within the meshed domain whereas $\boldsymbol{\rho} = \left\{ d_1 \quad \dots \quad \rho_e \quad \dots \quad \rho_{n_f} \right\}$ represents the set of design variables with lower and upper bounds $\boldsymbol{\rho}_\ell$ and $\boldsymbol{\rho}_u$, respectively. Moreover, $\mathbf{K}$ and $\mathbf{u}$ are global stiffness matrix and static displacements vector, respectively. The constrain in Eq. (1) ensures that the volume of the final optimal solution does not exceed a threshold value equal to V_{max}.

In order to formulate the topology optimization for dynamic problems, a linear viscous elastic structure is assumed according to the Rayleigh damping model:

$$\mathbf{C} = a_0 \mathbf{M} + a_1 \mathbf{K}, \tag{2}$$

where $\mathbf{M}$ is the constant global mass matrix whereas a_0 and a_1 are two positive constants calculated by imposing that the damping ratio ξ_s is the same for the first two modes of the structure. Therefore, the following relationships hold:

$$a_0 = \xi_s \frac{2\omega_1 \omega_2}{\omega_1 + \omega_2}, \tag{3a}$$

$$a_1 = \xi_s \frac{2}{\omega_1 + \omega_2}, \tag{3b}$$

where ω_1 and ω_2 are the first two circular natural frequencies of the structure. If the structural system is subjected to a seismic ground acceleration $\ddot{u}_g$ within the time window $[0, t_f]$, then the motion equation reads:

$$\ddot{\mathbf{u}} + \mathbf{M}^{-1}\mathbf{C}\dot{\mathbf{u}} + \mathbf{M}^{-1}\mathbf{K}\mathbf{u} = -\mathbf{r}\ddot{u}_g, \tag{4}$$

where $\mathbf{u}$ are now the dynamic displacements of the structure, $\mathbf{r}$ is the incidence vector and the dots indicate the derivative with respect to time. Formally, the statement of the topology optimization problem for dynamical systems can thus be expressed by rearranging the static compliance problem in Equation (1) as follows:

$$\begin{aligned} &\min_{\boldsymbol{\rho}} \left\{ \int_0^{t_f} \mathbf{u}^\top \mathbf{K} \mathbf{u} \mathrm{d}t \right\} \\ &\text{s.t.} \\ &\sum_{e=1}^{n_f} V_e = V_{max} \\ &\boldsymbol{\rho}_\ell \leq \boldsymbol{\rho} \leq \boldsymbol{\rho}_u. \end{aligned} \tag{5}$$

3 OPTIMUM DESIGN FOR STOCHASTIC SEISMIC LOADING

The topology optimization problem for structures subjected to stationary stochastic seismic loading is now discussed. The seismic ground motion model is a filtered white Gaussian noise, and the structural system dynamics is described using the state-space representation. Once the covariance matrix of the stochastic response is obtained, the topology optimization problem is presented.

3.1 Stochastic seismic excitation model

Random vibration theory allows to assess the probabilistic response of dynamical systems under random dynamic loads without the need of performing extensive Monte Carlo simulations based on direct integration of the motion equations. This makes random vibration theory especially attractive for topology optimization of large structures under dynamic loads characterized by inherent randomness. Therefore, the seismic ground motion $\ddot{u}_g$ is herein modeled as a stationary filtered white Gaussian noise through the Clough-Penzien filter as follows:

$$\ddot{u}_g = \mathbf{a}_p^\top \mathbf{z}_p, \tag{6a}$$

$$\dot{\mathbf{z}}_p = \mathbf{D}_p \mathbf{z}_p + \mathbf{v}_p W, \tag{6b}$$

where

$$\mathbf{a}_p = \left\{ -\omega_p^2 \quad -2\xi_p\omega_p \quad \omega_k^2 \quad 2\xi_k\omega_k \right\}^\top, \tag{7a}$$

$$\mathbf{z}_p = \left\{ u_p \quad \dot{u}_p \quad u_k \quad \dot{u}_k \right\}^\top, \tag{7b}$$

$$\mathbf{D}_p = \begin{bmatrix} 0 & 1 & 0 & 0 \\ -\omega_p^2 & -2\xi_p\omega_p & \omega_k^2 & 2\xi_k\omega_k \\ 0 & 0 & 0 & 1 \\ 0 & 0 & -\omega_k^2 & -2\xi_k\omega_k \end{bmatrix}, \tag{7c}$$

$$\mathbf{v}_p = \left\{ 0 \quad 0 \quad 0 \quad -1 \right\}^\top. \tag{7d}$$

where ω_p and ξ_p, ω_k and ξ_k are the filter parameters whereas W is a zero-mean white Gaussian noise having constant power spectral density S_0. It is evaluated as function of the peak ground acceleration $\ddot{u}_g^{max}$ according to the following relationship:

$$S_0 = \frac{\left(\ddot{u}_g^{max}\right)^2}{\gamma^2 \left[\pi\omega_k \left(2\xi_k + \dfrac{1}{2\xi_k} \right) \right]}, \tag{8}$$

where $\gamma = 2.8$ denotes the peak factor, see for instance Liu et al. [20].

3.2 Covariance analysis

By assembling the equation of motion in Eq. (4) and the filter equation in Eq. (6), the state-space representation of the overall dynamics is obtained as follows:

$$\underbrace{\begin{Bmatrix} \dot{\mathbf{z}}_s \\ \dot{\mathbf{z}}_p \end{Bmatrix}}_{\dot{\mathbf{z}}} = \underbrace{\begin{bmatrix} \mathbf{A}_s & \mathbf{H}_p \\ \mathbf{0}_{4\times 2n_d} & \mathbf{D}_p \end{bmatrix}}_{\mathbf{A}} \underbrace{\begin{Bmatrix} \mathbf{z}_s \\ \mathbf{z}_p \end{Bmatrix}}_{\mathbf{z}} + \underbrace{\begin{Bmatrix} \mathbf{0}_{2n_d\times 1} \\ \mathbf{v}_p W \end{Bmatrix}}_{\mathbf{f}}, \tag{9}$$

where

$$\mathbf{z}_s = \left\{ \mathbf{u} \quad \dot{\mathbf{u}} \right\}^\top, \tag{10}$$

$$\mathbf{A}_s = \begin{bmatrix} \mathbf{0}_{n_d} & \mathbf{I}_{n_d} \\ -\mathbf{M}^{-1}\mathbf{K} & -\mathbf{M}^{-1}\mathbf{C} \end{bmatrix}, \tag{11}$$

$$\mathbf{H}_p = \left[\mathbf{0}_{n_d \times 4} \quad -\mathbf{r}\mathbf{a}_p^\top \right]^\top, \tag{12}$$

while $\mathbf{0}$ is a (square or rectangular) null matrix or vector and $\mathbf{I}$ is the (square) identity matrix, respectively (their size is explicated in the corresponding subscripts, where a single number is used for a square matrix). Given this state-space representation, the response covariance matrix of the resulting linear time-invariant system is defined as follows:

$$\mathbf{R} = \mathrm{E}\left[\mathbf{z}\mathbf{z}^\top\right] = \mathrm{E}\left[\begin{Bmatrix} \mathbf{z}_s \\ \mathbf{z}_p \end{Bmatrix} \begin{Bmatrix} \mathbf{z}_s & \mathbf{z}_p \end{Bmatrix} \right] = \begin{bmatrix} \mathbf{R}_{\mathbf{z}_s\mathbf{z}_s} & \mathbf{R}_{\mathbf{z}_s\mathbf{z}_p} \\ \mathbf{R}_{\mathbf{z}_p\mathbf{z}_s} & \mathbf{R}_{\mathbf{z}_p\mathbf{z}_p} \end{bmatrix}, \tag{13}$$

where

$$\mathbf{R}_{\mathbf{z}_s\mathbf{z}_s} = \begin{bmatrix} \mathbf{R}_{\mathbf{u}\mathbf{u}} & \mathbf{R}_{\mathbf{u}\dot{\mathbf{u}}} \\ \mathbf{R}_{\dot{\mathbf{u}}\mathbf{u}} & \mathbf{R}_{\dot{\mathbf{u}}\dot{\mathbf{u}}} \end{bmatrix}. \tag{14}$$

The matrix $\mathbf{R}$, in turn, is the solution of the Lyapunov equation in stationary conditions, which reads:

$$\mathbf{A}\mathbf{R} + \mathbf{R}\mathbf{A}^\top + \mathbf{B} = \mathbf{0}_{2n_d+4 \times 2n_d+4}, \tag{15}$$

where $\mathbf{B}$ is a matrix whose elements are equal to zero expect that the element whose index is $(2n_d + 4, 2n_d + 4)$, which is equal to $2\pi S_0$.

3.3 Optimum design under stochastic seismic loads

By applying the mean value operator $\mathrm{E}[\cdot]$ to the objective function $\mathcal{F}$ of the optimization problem formulated in Eq. (5), it can be found that:

$$\mathrm{E}\left[\mathcal{F}\right] = \mathrm{E}\left[\int_0^T \mathbf{u}^\top \mathbf{K} \mathbf{u} \mathrm{d}t \right] = \int_0^T \mathbf{r}^\top \left(\mathbf{K} \otimes \mathbf{R}_{\mathbf{u}\mathbf{u}} \right) \mathbf{r} \mathrm{d}t, \tag{16}$$

where $\otimes$ is the term-by-term product and $\mathbf{R}_{\mathbf{u}\mathbf{u}}$ is the covariance matrix of the structural displacements (i.e., the square block of size $n_d \times n_d$ of the matrix $\mathbf{R}$ in Eq. (14) whose elements index lies between 1 and n_d). Hence, by recalling that a stationary ground motion is here assumed, the topology optimization problem in Eq. (5) can be simplified as follows:

$$\begin{aligned} &\min_{\boldsymbol{\rho}} \left\{ \mathbf{r}^\top \left(\mathbf{K} \otimes \mathbf{R}_{\mathbf{u}\mathbf{u}} \right) \mathbf{r} \right\} \\ &\quad \text{s.t.} \\ &\quad \sum_{e=1}^{n_f} V_e = V_{max} \\ &\quad \boldsymbol{\rho}_\ell \leq \boldsymbol{\rho} \leq \boldsymbol{\rho}_u \end{aligned} \tag{17}$$

4 COMPUTATIONAL ISSUES

4.1 Topology design via Solid Isotropic Material with Penalization

The Solid Isotropic Material with Penalization (SIMP) approach is adopted in this work in order to find efficiently the optimal solution for the topology optimization problem formulated in Eq. 17. The computational procedure starts with a spatial discretization of the continuum design domain. The SIMP approach [21] is thus performed by assuming that the design variable is constant over the finite element with a resulting uniform distribution of the structural material. The mechanical properties of each element are determined using a heuristic power-law interpolation that relates the element-wise design variable with the element elastic properties as follows:

$$E_e(\rho_e) = \rho_e^p E_0 \text{ with } \rho_{min} \leq \rho_e(d_j) \leq 1, \tag{18}$$

where E_0 is the elastic modulus of the base material and ρ_{min} is a non-zero minimum value for $\rho_e(d_j)$ that serves at preventing the singularity of the stiffness matrix. A coefficient $p > 1$ is introduced to penalize the presence of intermediate densities in the relaxed setting and steer the solution to discrete integer values (i.e., black-and-white digital image).

It is well recognized that topology optimization problems are especially sensitive to numerical instabilities, which are related to the possible non-existence/non-uniqueness of the optimal solution as well as to the lack of convergence, thereby resulting in some anomalies into the final design. The presence of checkerboarding, mesh dependence and local minima makes the interpretation of the optimal layout unfeasible and should be avoided by adopting a proper regularization scheme. To circumvent the occurrence of such problems, the density-filter proposed in [22] is adopted in the present work. It relies on the convolution product between a filter kernel and the design density vector, which leads to:

$$\rho_e(d_j) = \frac{\sum_{j \in \mathcal{N}_e} H_{ej} d_j}{\sum_{j \in \mathcal{N}_e} H_{ej}}, \tag{19}$$

where H_{ej} are weighting functions defined through a linearly decaying function of fixed-length radius r_{min}. The linear density filter function modifies the densities of the element e to be a function of the design variable d_j and of its neighborhood $\mathcal{N}_e$.

Because the density variable is assumed to be constant over each finite element, the relationship in Eq. (18) can be implemented for the finite element stiffness matrix by simply scaling it before the global stiffness matrix is assembled. The finite element stiffness matrix is interpolated and expressed in terms of E_0 as follows:

$$\mathbf{K}_e\left(\rho_e\right) = E_e(\rho_e)\mathbf{K}_e^0 = \rho_e^p \mathbf{K}_e^0, \tag{20}$$

where $\mathbf{K}_e^0$ is the finite element stiffness matrix with unit elastic modulus. The adoption of the SIMP approach is particularly beneficial if implemented in iterative algorithms since it allows calculating the finite element stiffness matrices at the beginning of the procedure. For each loop, finite element stiffness matrices are simply updated using the fictitious elasticity modulus E_e and then assembled to solve for the system covariance matrix.

4.2 SENSITIVITY ANALYSIS

The derivative of the objective function f in Eq. (17) with respect to the design variable ρ_e is:

$$\frac{\partial f}{\partial \rho_e} = \mathbf{r}^\top \left(\frac{\partial \mathbf{K}}{\partial \rho_e} \otimes \mathbf{R_{uu}} \right) \mathbf{r} + \mathbf{r}^\top \left(\mathbf{K} \otimes \frac{\partial \mathbf{R_{uu}}}{\partial \rho_e} \right) \mathbf{r}. \tag{21}$$

For this preliminary study, a direct differentiation approach is adopted. The calculation of the derivatives $\partial \mathbf{R}_{\mathbf{uu}}/\partial \rho_e$ requires the solution of the following associate stationary Lyapunov equation:

$$\mathbf{A}\frac{\partial \mathbf{R}}{\partial \rho_e} + \frac{\partial \mathbf{R}}{\partial \rho_e}\mathbf{A}^\top + \bar{\mathbf{B}} = \mathbf{0}_{2n_d+4\times 2n_d+4} \text{ for } e = 1, \ldots, n_f, \tag{22}$$

with

$$\bar{\mathbf{B}} = \frac{\partial \mathbf{A}}{\partial \rho_e}\mathbf{R} + \mathbf{R}\frac{\partial \mathbf{A}^\top}{\partial \rho_e}. \tag{23}$$

It is also noted that:

$$\frac{\partial \mathbf{A}}{\partial \rho_e} = \begin{bmatrix} \dfrac{\partial \mathbf{A}_s}{\partial \rho_e} & \mathbf{0}_{2n_d\times 4} \\ \mathbf{0}_{4\times 2n_d} & \mathbf{0}_4 \end{bmatrix}, \tag{24}$$

in which

$$\frac{\partial \mathbf{A}_s}{\partial \rho_e} = \begin{bmatrix} \mathbf{0}_{n_d} & \mathbf{0}_{n_d} \\ \mathbf{M}^{-1}\dfrac{\partial \mathbf{M}}{\partial \rho_e}\mathbf{M}^{-1}\mathbf{K} - \mathbf{M}^{-1}\dfrac{\partial \mathbf{K}}{\partial \rho_e} & \mathbf{M}^{-1}\dfrac{\partial \mathbf{M}}{\partial \rho_e}\mathbf{M}^{-1} - \mathbf{M}^{-1}\dfrac{\partial \mathbf{C}}{\partial \rho_e} \end{bmatrix}. \tag{25}$$

The derivative of $\mathbf{C}$ with respect to ρ_e is calculated as follows:

$$\frac{\partial \mathbf{C}}{\partial \rho_e} = \frac{\partial a_0}{\partial \rho_e}\mathbf{M} + a_0\frac{\partial \mathbf{M}}{\partial \rho_e} + \frac{\partial a_1}{\partial \rho_e}\mathbf{K} + a_1\frac{\partial \mathbf{K}}{\partial \rho_e}, \tag{26}$$

where

$$\frac{\partial a_0}{\partial \rho_e} = \frac{\partial a_0}{\partial \omega_1}\frac{\partial \omega_1}{\partial \rho_e} + \frac{\partial a_0}{\partial \omega_2}\frac{\partial \omega_2}{\partial \rho_e}, \tag{27a}$$

$$\frac{\partial a_1}{\partial \rho_e} = \frac{\partial a_1}{\partial \omega_1}\frac{\partial \omega_1}{\partial \rho_e} + \frac{\partial a_1}{\partial \omega_2}\frac{\partial \omega_2}{\partial \rho_e}. \tag{27b}$$

The derivatives of the constants a_0 and a_1 with respect to ρ_e are calculated as follows:

$$\frac{\partial a_0}{\partial \omega_1} = \frac{2\xi_s\omega_2^2}{(\omega_1+\omega_2)^2}, \quad \frac{\partial a_0}{\partial \omega_2} = \frac{2\xi_s\omega_1^2}{(\omega_1+\omega_2)^2}, \tag{28}$$

$$\frac{\partial a_1}{\partial \omega_1} = \frac{-2\xi_s}{(\omega_1+\omega_2)^2}, \quad \frac{\partial a_1}{\partial \omega_2} = \frac{-2\xi_s}{(\omega_1+\omega_2)^2}, \tag{29}$$

whereas

$$\frac{\partial \omega_1}{\partial \rho_e} = \frac{1}{2\omega_1}\frac{\partial \lambda_1}{\partial \rho_e}, \quad \frac{\partial \omega_2}{\partial \rho_e} = \frac{1}{2\omega_2}\frac{\partial \lambda_2}{\partial \rho_e} \tag{30}$$

are the derivatives of the first two circular natural frequencies of the structure. The terms λ_1 and λ_2 are the first two eigenvalues of the following eigenproblem:

$$\boldsymbol{\phi}_k^\top \mathbf{K}\phi_k = \lambda_k \boldsymbol{\phi}_k^\top \mathbf{M}\boldsymbol{\phi}_k, \tag{31}$$

in which $\boldsymbol{\phi}_k$ is the kth eigenvector. The derivatives of λ_1 and λ_2 with respect to ρ_e are evaluated as follows:

$$\frac{\partial \lambda_1}{\partial \rho_e} = \boldsymbol{\phi}_1^\top \left[\frac{\partial \mathbf{K}}{\partial \rho_e} - \lambda_1\frac{\partial \mathbf{M}}{\partial \rho_e}\right]\boldsymbol{\phi}_1, \quad \frac{\partial \lambda_2}{\partial \rho_e} = \boldsymbol{\phi}_2^\top \left[\frac{\partial \mathbf{K}}{\partial \rho_e} - \lambda_2\frac{\partial \mathbf{M}}{\partial \rho_e}\right]\boldsymbol{\phi}_2, \tag{32}$$

under the assumption of distinct real eigenvalues and the mass orthonormalization condition.

Finally, by virtue of the SIMP method, it is obtained that:

$$\frac{\partial \mathbf{K}}{\partial \rho_e} = \bigwedge_{e=1}^{n_f} \frac{\partial \mathbf{K}_e}{\partial \rho_e} = \bigwedge_{e=1}^{n_f} p\rho_e^{p-1}\mathbf{K}_{e,0}, \tag{33a}$$

$$\frac{\partial \mathbf{M}}{\partial \rho_e} = \bigwedge_{e=1}^{n_f} \frac{\partial \mathbf{M}_e}{\partial \rho_e} = \bigwedge_{e=1}^{n_f} q\rho_e^{q-1}\mathbf{M}_{e,0}, \tag{33b}$$

where $\bigwedge$ stands for standard finite element assembly operator.

5 EFFECTS OF SEISMIC MASS MODELING ON FINAL TOPOLOGIES

In seismic topology design of structural systems, the dynamic load is design-dependent because the inertial load is function of position and value of the structural mass within the domain. In order to obtain objective, reliable, and feasible optimal solutions, a proper modeling of the seismic mass is, therefore, of primary importance and deserves a thorough understanding. Some examples are discussed in such a way to highlight the significance of the mass modeling assumptions on the final topologies.

The reference model is based on a two-dimensional domain with single bay and high equal to 5 m and 15 m, respectively. The inter-story height is equal to 5 m, thereby resulting in three levels along the building elevation. The floors are made of concrete decks and their mass is calculated considering dead and live loads equal to 7.0 kN/m^2 and 2.0 kN/m^2, respectively. The design domain is discretized using 4-node quadrilateral Lagrangian (Q4) elements with a uniform thickness equal to 0.15 m and a mesh size 0.25 m $\times$ 0.25 m (which implies a total of 1,200 finite elements). The continuum domain is modeled using steel as building material, with elastic modulus $E_0 = 210$ GPa. The algorithm is executed with constant penalization factor $p = 3$, projection radius $r_{min} = 0.3$ m and initial volume fraction over the Q4 domain equal to 30%. The Rayleigh damping model is assumed with damping ratio equal to 5%. Fixed supports are considered at the base and a symmetry constraint with respect to the centerline is enforced. A seismic ground motion with $\ddot{u}_g^{max} = 0.3g$ is assumed, with $\xi_p = \xi_k = 0.6$, $\omega_p = 1.5$ rad/s and $\omega_k = 15$ rad/s.

A complete system is fully defined by combining the continuum domain with the discrete elements of the gravity load-bearing frame, as already proposed in previous works [2, 23]. The introduction of a non-designable secondary system improves the feasibility of the final solution (e.g., clearer identification of the working points, disappearance of small multiple horizontal elements) and makes the topological results independent from the direct application of the external load on the domain, whether it is static or dynamic. For a deeper understanding of the role of the secondary systems and symmetry constraints on optimal topologies of lateral resisting systems for tall buildings, the reader is referred to the work by Angelucci et al. [15].

For the seismic design of tall buildings, and multi-story buildings in general, the structural mass of the system $\mathbf{M}$ can be decomposed into two contributions $\mathbf{M} = \mathbf{M}_f + \mathbf{M}_\Omega$, where $\mathbf{M}_f$ is the seismic mass of the building components estimated by considering the floor tributary areas and $\mathbf{M}_\Omega$ is the mass of the designable lateral resisting system. Nevertheless, it is straightforward to recognize that, in multi-story buildings and especially for concrete slabs, the mass is primarily located at the floor levels and the lateral resisting system contributes only for a small fraction of the overall building mass. Since the seismic excitation produces inertial forces mostly associated with the tributary mass of the building $\mathbf{M}_f$, the introduction of the

floor mass within the optimizable domain is incorrect from a conceptual standpoint. During the optimization routines, in fact, the dynamic characteristics of the domain representing the lateral resisting system are iteratively updated according to the new material distribution and the inherent structural mass is partially removed. Additionally, it can be demonstrated that when the seismic mass is included in the designable domain, updating the mass arrangement at each iteration slows down the rate of convergence and compromises the stability of the whole topology optimization procedure. Therefore, it is required to allocate the tributary mass within a non-optimizable domain, which remains constant during the optimization routines and expediently relaxes the design-dependency of the tributary mass on the element variables (i.e., $\partial \mathbf{M}_f / \partial \rho_e$ is null). Moreover, since the weight of the bracing members is negligible compared to the mass of the story levels, it is possible to assume a massless optimizable domain in the seismic analysis, without any significant loss of accuracy. The structural mass is thus kept constant during the iterative process, and this allows to state that the final topologies are almost exclusively dependent on the stiffness properties of the continuum elements. Within the scope of this work, the tributary mass is located at each floor level in the horizontal direction only, provided that the dynamic excitation does not include external forces at the nodes in the vertical and rotational degrees of freedom.

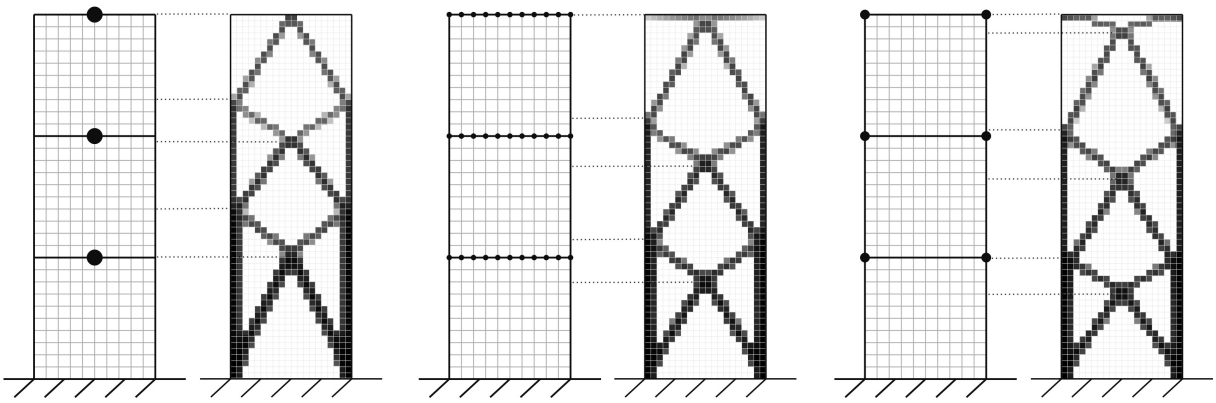

Figure 1: Reference models and optimal topologies for different mass modelling: lumped mass at the floor diaphragms (a, b); distributed mass at story levels (c, d); lumped mass at master nodes (e, f).

In the analysis and design of tall buildings subjected to lateral loads, floor slabs are usually assumed to possess high in-plane stiffness, and the assumption of diaphragm constraints reflects quite well the real behavior. This assumption justifies the concentration of the structural mass in a single point at each floor as illustrated in Figure 1a, and allows to further reduce the degrees of freedom of the structural system, thereby simplifying the seismic analysis. However, in case of topology optimization, the introduction of a displacement constraint undermines the objectivity of the final solution because the rigidity/flexibility of the floor diaphragms has a significant influence on the building model. As illustrated in Figure 1b, the optimized layout shows a design-dependent topology, where the diagonal arrangement of the lateral resisting system is affected by the specific location of the tributary mass in the middle of each story level.

Since rigid diaphragm constraints lead to flawed solutions, the effects of floor deformability cannot be disregard and a reasonable stiffness must be assigned to each floor. Figure 1c illustrates the designable and non-designable domains of the reference model, in which the tributary mass is uniformly distributed at the floor levels. The beams are discretized into smaller ele-

ments, which allows the mass nodes to be coincident with the interior joints of the quadrilateral mesh. The optimal layout presented in Figure 1d results in a K-brace arrangement at the top of the building, due to the development of inertial forces along the line. The top member, in fact, is needed to transfer the load along the bay between the far sided columns. Although correct from a topological standpoint, this solution is theoretically inaccurate since the presence of floor beams at each story level contributes to transmit gravity loads to the vertical members of the unbraced frame. The reference model is thus modified accordingly to reduce the tributary mass to a discrete number of master nodes of the floor system located at the intersections of the secondary system (extreme corners of the quadrilateral mesh in Figure 1e). The resulting topology in Figure 1f shows the optimal solution where theoretical concepts and modeling assumptions are both fulfilled.

Because inertial loads originate at master nodes of the secondary system only and assuming that the auxiliary perimeter framework is not included in the optimizable domain, the final topologies are independent from the master nodes definition. This allows to choose arbitrarily the secondary system bounding the continuum domain. Additionally, the distribution of the seismic mass at a discrete number of nodes suggests the adoption of a reduced-order model during the dynamic analysis of the structural system. Through static condensation, stiffness and mass matrices (and implicitly the damping matrix) of the complete system can be properly reduced to the degrees of freedom of the master nodes.

The demanding computational cost of the dynamic topology optimization process certainly benefits from the sub-structuring technique, where inversion and eigenanalysis of large-size matrices are generally involved. Without any loss of objectivity, the eigenvalue analysis can be performed on the reduced-order system since natural frequencies and modal shapes are defined at the master node locations only.

6 CASE STUDY

The topology optimization problem is solved next to define the lateral resisting system of a multi-story building subjected to ground motion excitation. Particularly, given a stationary-type support excitation described as filtered white Gaussian noise, the optimal material distribution is attained by minimizing the dynamic compliance in the continuum design domain under a volume constraint. The reference model is a regular multi-story building with height and width equal to 40 m and 20 m, respectively. The external skin of the building is split into four panels, such that each façade can be analyzed as a continuous optimizable design domain discretized by using Q4 elements with uniform thickness equal to 0.15 m. A two-dimensional case study is deemed accurate enough. The structure is idealized with fixed supports and symmetry constraints are imposed.

An auxiliary load-bearing framework bounding the continuum domain is designed with bay width and inter-story height equal to 5 m and 4 m, respectively. W8x21 steel cross-sections are preliminary designed to model columns and beams of the unbraced frame, which is considered as a non-designable domain during the optimization process. The frame members are discretized into smaller elements, so that the nodes of the beam-column elements (thick black lines in Figure 2) and those of the Q4 elements (grid area in Figure 2) coincide each other. This operation results in a continuous connection between the discrete frame and the continuum domain throughout height and width of the building. Floor slabs are placed every 4 m. The associated seismic mass is calculated considering gravity loads equal to 9.0 kN/m^2 and tributary influence areas. The floor mass is lumped at the master nodes at 5 locations for each floor level, corresponding to the intersection of floor beam and column lines (black nodes in Figure

2). The algorithm is executed once again with constant penalization factor $p = 3$, projection radius $r_{min} = 0.3$ m and initial volume fraction over the Q4 domain equal to 30%.

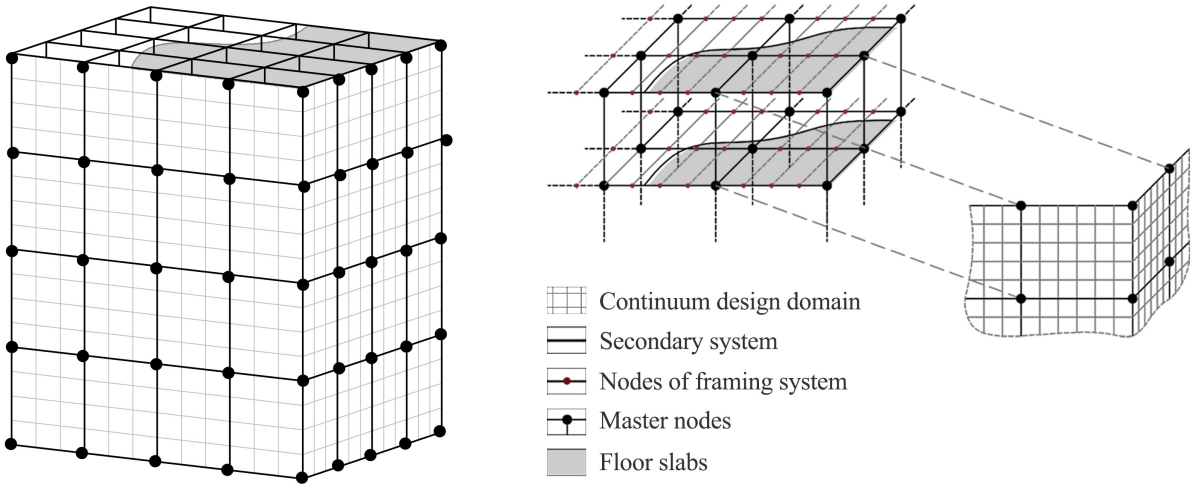

Figure 2: Schematic of the constitutive elements of the numerical model.

The topology optimization is first performed for the reference model with unit mesh size (1 m $\times$ 1 m, resulting in 800 finite elements). The optimal topology is displayed in Figure 3b in terms of filtered design variables. Figure 3c shows the optimal layout obtained when refining the design domain using a mesh size equal to 0.5 m $\times$ 0.5 m (total of 3,200 finite elements). The results clearly demonstrate that the optimal topologies are qualitatively the same, with the possible exception of major differences at the domain boundaries, which become gradually smoother with the mesh refinement. The material distribution within the design domain assumes a precise arrangement composed by two lateral columns and two pairs of full-width diagonal braces. The optimized domain is post-processed to physically appreciate the results of the topology optimization process and correctly identify the location of the working points of brace-to-brace and brace-to-column nodes. It is worth noticing here that the optimal topology does not include the presence of a secondary framed system (which is constituted by intermediate beams and columns), and thus it can be omitted from the final layout. The evolution of the optimal solution during the optimization routines is illustrated in Figure 4 by plotting objective function (dynamic compliance) and constraint function (material volume) values with respect to the number of iterations required until a tolerance of 1% is met (the filled circle marks the convergence). The efficiency of the topology optimization framework is confirmed by the steady convergence as well as the limited number of iterations.

7 CONCLUSIONS

The minimum compliance formulation for the topology optimization of large structures under seismic excitation has been discussed in this work. The huge computational effort required, even for the case of linear elastic systems, has made the adoption of classical time-history dynamic analyses prohibitive. To overcome this challenge and deal with the topology optimization of tall buildings under seismic loads, random vibration theory has been explored in this study. The well-posedness of the optimization problem has been ensured through the adoption of the SIMP approach. A sensitivity analysis of the objective function with respect to the ele-

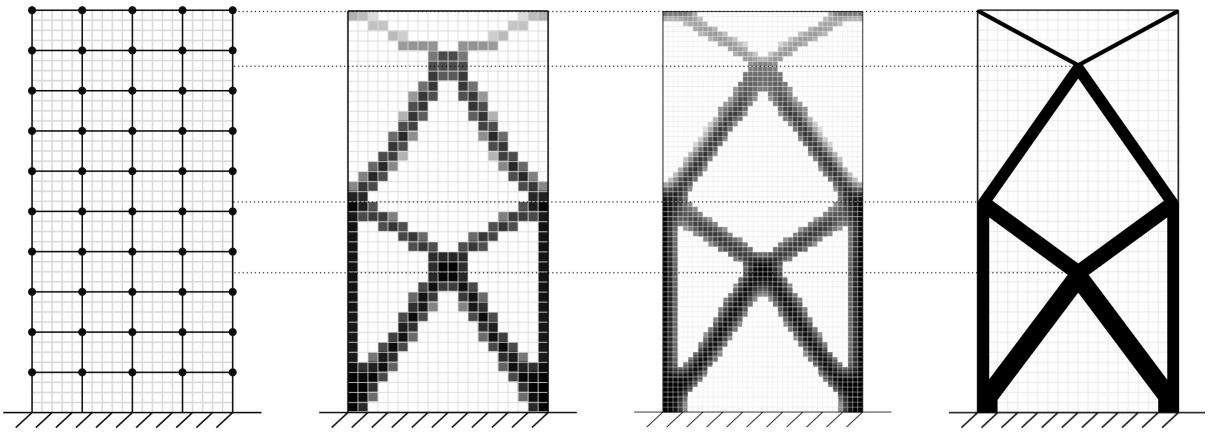

Figure 3: Reference model of the 40 m $\times$ 20 m tall building (a), optimal topologies for mesh sizes 1 m $\times$ 1 m (b) and 0.5 m $\times$ 0.5 m (c), post-processed refined layout (d).

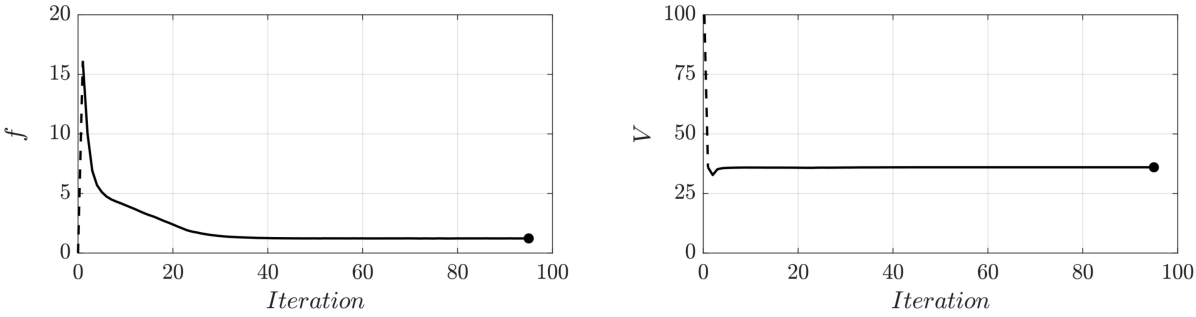

Figure 4: Objective function (left) and constraint function (right) value for mesh size 1 m $\times$ 1 m.

ment design variables has been assessed analytically to foster the employment of gradient-based methods.

The present study has paid special attention to mass modeling techniques for tall buildings under earthquakes within topology optimization procedures. Numerical examples have been presented to validate the effects of preliminary theoretical assumptions on the final layouts. Finally, a paradigmatic case study has been discussed to demonstrate effectiveness and stability of the proposed framework in finding the optimum solutions. A gradually refined mesh process has been also presented to explore the efficiency of the optimization procedure in avoiding numerical mesh-dependency instabilities.

The findings presented here should be considered as a first attempt toward the development of more sophisticated dynamic formulations within topology optimization frameworks. Further improvements and extensions will be included in future works to identify optimal lateral resisting systems for multi-story buildings subjected to stochastic processes, where fully non-stationary models will be considered to simulate the seismic ground motion more accurately.

REFERENCES

[1] O. Sigmund, A 99 line topology optimization code written in Matlab. *Structural and Multidisciplinary Optimization*, **21**(2), 120–127, 2001.

[2] L.L. Stromberg, A. Beghini, W.F. Baker, G.H. Paulino, Topology optimization for braced frames: combining continuum and beam / column elements. *Engineering Structures*, **37**, 106–124, 2012.

[3] C. Talischi, G.H. Paulino, A. Pereira, I.F.M. Menezes, PolyTop: a Matlab implementation of a general topology optimization framework using unstructured polygonal finite element meshes. *Structural and Multidisciplinary Optimization*, **45**(3), 329-357, 2012.

[4] K. Liu, A. Tovar, An efficient 3D topology optimization code written in Matlab. *Structural and Multidisciplinary Optimization*, **50**(6), 1175–1196, 2014.

[5] G. Angelucci, S.M.J. Spence, F. Mollaioli, An integrated topology optimization framework for three-dimensional domains using shell elements. *Structural Design of Tall and Special Buildings*, **30**(1), 1–17, 2021.

[6] A.R. Díaaz, N. Kikuchi, Solutions to shape and topology eigenvalue optimization problems using a homogenization method. *International Journal for Numerical Methods in Engineering*, **35**(7), 1487–1502, 1992.

[7] A.P. Seyranian, E. Lund, N. Olhoff, Multiple eigenvalues in structural optimization problems. *Structural Optimization*, **8**(4), 207–227, 1994.

[8] N.L. Pedersen, Maximization of eigenvalues using topology optimization. *Structural and Multidisciplinary Optimization*, **20**(1), 2–11, 2000.

[9] G.H. Yoon, Structural topology optimization for frequency response problem using model reduction schemes. *Computer Methods in Applied Mechanics and Engineering*, **199**(25–28), 1744–1763, 2010.

[10] S. Min, N. Kikuchi, Y.C. Park, S. Kim, S. Chang, Optimal topology design of structures under dynamic loads. *Structural Optimization*, **17**(2–3), 208–218, 1999.

[11] Y. Maeda, S. Nishiwaki, K. Izui, M. Yoshimura, K. Matsui, K. Terada, Structural topology optimization of vibrating structures with specified eigenfrequencies and eigenmode shapes. *International Journal for Numerical Methods in Engineering*, **67**(5), 597–628, 2006.

[12] E.T. Filipov, J. Chun, G.H. Paulino, J. Song, Polygonal multiresolution topology optimization (PolyMTOP) for structural dynamics. *Structural and Multidisciplinary Optimization*, **53**(4), 673–694, 2016.

[13] W.H. Greene, R.T. Haftka, Computational aspects of sensitivity calculations in linear transient structural analysis. *Structural Optimization*, **3**(3), 176–201, 1991.

[14] J. Zhao, C. Wang, Dynamic response topology optimization in the time domain using model reduction method. *Structural and Multidisciplinary Optimization*, **53**(1), 101–114, 2016.

[15] G. Angelucci, F. Mollaioli, O. AlShawa, Evaluation of optimal lateral resisting systems for tall buildings subject to horizontal loads. *Procedia Manufacturing*, **44**, 457–464, 2020.

[16] Y. Yang, M. Zhu, M.D. Shields, J.K. Guest, Topology optimization of continuum structures subjected to filtered white noise stochastic excitations. *Computer Methods in Applied Mechanics and Engineering*, **324**, 438–456, 2017.

[17] M. Zhu, Y. Yang, J.K. Guest, M.D. Shields, Topology optimization for linear stationary stochastic dynamics: applications to frame structures. *Structural Safety*, **67**, 116–131, 2017.

[18] J. Chun, J. Song, G.H. Paulino, System-reliability-based design and topology optimization of structures under constraints on first-passage probability. *Structural Safety*, **76**, 81–94, 2019.

[19] B.S. Kang, G.J. Park, J.S. Arora, A review of optimization of structures subjected to transient loads. *Structural and Multidisciplinary Optimization*, **31**(2), 81–95, 2006.

[20] Z. Liu, W. Liu, Y. Peng, Random function based spectral representation of stationary and non-stationary stochastic processes. *Probabilistic Engineering Mechanics*, **45**, 115–126, 2016.

[21] M.P. Bendsøe, O. Sigmund, Material interpolation schemes in topology optimization. *Archive of Applied Mechanics*, **69**(9), 635–654, 1999.

[22] B. Bourdin, Filters in topology optimization. *International journal for numerical methods in engineering*, **50**(9), 2143–2158, 2001.

[23] S. Bobby, S.M. Spence, A. Kareem, Data-driven performance-based topology optimization of uncertain wind-excited tall buildings. *Structural and Multidisciplinary Optimization*, **54**(6), 1379–1402, 2016.